

Start-up of flow of a FENE-fluid through a 4:1:4 constriction in a tube

P. Szabo ¹, J.M. Rallison, E.J. Hinch *

*Department of Applied Mathematics and Theoretical Physics, University of Cambridge, Silver Street,
Cambridge CB3 9EW, UK*

Received 14 November 1996; received in revised form 20 February 1997

Abstract

The flow of a FENE-fluid through a 4:1:4 constriction in a tube is computed by a split Lagrangian–Eulerian finite element method. In steady flow it is found that the upstream vortex grows with increasing Deborah number, while the down-stream vortex diminishes and disappears. The steady pressure drop decreases with Deborah number unless the finite extensibility L is quite small. Starting from rest at high Deborah number, the upstream vortex grows in two stages, each with their own time scales. A simple model of this growth is proposed. © 1997 Elsevier Science B.V.

Keywords: Viscoelastic flow; 4:1:4 contraction/expansion; FENE; Finite element method; Lagrangian formulation

1. Introduction

Elastic fluids resist converging flow through an orifice, responding by increasing the pressure drop and by forming strong vortices upstream which reduce the strain-rate. The benchmark flow to study this phenomenon is the 4:1 contraction between two channels or two tubes. We examine instead a 4:1:4 constriction in a tube. This has two advantages. First, the stress relaxes in a shorter distance downstream, not only because the divergence unwinds the upstream convergence but also because the flow is relatively slower. Hence one needs to compute a shorter distance downstream. Second, the total dissipation-rate is simply the flow-rate multiplied by the pressure drop, if the tube is sufficiently long for the elastic stress to return to the inlet state. A vibrational principle for the dissipation-rate therefore gives the pressure drop to good accuracy. As a further numerical convenience, we make the shape of the constriction round, in order to

* Corresponding author. Fax: +44 1223 337918.

¹ Present address: Department of Chemical Engineering, Technical University of Denmark, Building 227, DK-2800 Lyngby, Denmark.

eliminate the stress singularities at the sharp corners of the standard 4:1 contraction. Two different roundings are considered.

Experimentally, Cartalos and Piau [2] have studied the flow through a small orifice in a large plate between two reservoirs. They used HPAM and PEO solutions of low concentrations in viscous solvents. They observed a large vortex was formed upstream of the orifice. The size of the vortex downstream decreased with increasing flow-rate, and eventually disappeared. The pressure drop across the orifice increased significantly with the flow. Similar behaviour (except of course, for the downstream vortex) is seen experimentally in the benchmark 4:1 contraction (e.g. see McKinley, Raiford, Brown and Armstrong [6]).

This paper addresses the size of the upstream vortex and the pressure drop across the orifice. Previous numerical studies of flow through a 4:1 constriction (Marchal and Crochet [9]) and through an orifice into a tube (Keiller [7]) found for an Oldroyd-B fluid that the upstream vortex was small compared with experimental observations of viscoelastic fluids. Further they found that the pressure drop was smaller, rather than greater, than that of a Newtonian fluid having the same shear viscosity. Keiller identified the source of this pressure reduction as in the long exit pipe where the velocity profile relaxes to Poiseuille flow. Our 4:1:4 constriction does not have the long exit pipe. Keiller also found that FENE-fluids could produce a large upstream vortex.

We shall also be interested in how the upstream vortex is established when flow commences, and whether the rounding of the corner has any effect.

2. Governing equations

We consider axisymmetric flow along a circular tube with a 4:1:4 constriction, sketched in Fig. 1. Let the radius of the tube be R_u . The radius of the narrowest part of the constriction is then $R_c = \frac{1}{4}R_u$. The axial length of the constriction is R_c and the constriction shape is rounded so that in cylindrical coordinates we take two shapes

$$r = R_c \left(\frac{3}{2} - \frac{1}{2}(1 - (2z/R_c)^n)^{1/2} \right) \quad \text{in } |z| \leq \frac{1}{2}R_c,$$

with $n = 2$ for circular corners shown in Fig. 1, and $n = 4$ for sharper corners shown in Fig. 9.

The flow is taken to be incompressible and inertialess so that

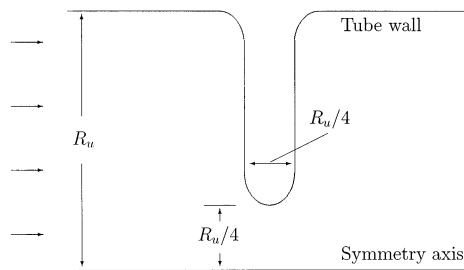


Fig. 1. The geometry of 4:1:4 constriction, with the $n = 2$ circular corners.

$$\nabla \cdot \mathbf{u} = 0, \quad (1)$$

$$\nabla \cdot \boldsymbol{\sigma} = 0. \quad (2)$$

We write the constitutive equation for a FENE-fluid in the form (Chilcott and Rallison [3]):

$$\boldsymbol{\sigma} = -p\mathbf{I} + 2\mu_s\mathbf{E} + Gf(\mathbf{A} - \mathbf{I}), \quad (3)$$

$$\frac{\partial \mathbf{A}}{\partial t} + \mathbf{u} \cdot \nabla \mathbf{A} - \mathbf{A} \cdot \nabla \mathbf{u} - \nabla \mathbf{u}^T \cdot \mathbf{A} = -\frac{f}{\tau}(\mathbf{A} - \mathbf{I}), \quad (4)$$

where \mathbf{E} is the rate of strain, μ_s the solvent viscosity, G an elastic modulus, τ the relaxation time, and the FENE factor with finite extensibility L is

$$f = \frac{L^2}{L^2 - \text{trace}(\mathbf{A})}. \quad (5)$$

In this form, the fluid has a constant viscosity $\mu_s + G\tau$ in steady shear flow.

Boundary conditions of no slip are applied on the solid surfaces, and Poiseuille flow far up and downstream at $z = \pm 5R_u$. The inlet condition for \mathbf{A} corresponds to steady Poiseuille flow. Elsewhere in the flow, initial conditions of $\mathbf{A} = \mathbf{I}$ are used.

The problem is non-dimensionalised as follows. Lengths are scaled on the tube radius R_u . With volume flux Q along the tube, velocities are scaled on the average upstream velocity $Q/\pi R_u^2$. Note that the average velocity in the constriction will be 16 times higher. From these length and velocity scales we obtain the time scale of the flow as $\pi R_u^3/Q$. The Deborah number for the flow upstream De_u is then the ratio of the relaxation time τ to this flow time scale. As all the phenomena of interest, however, take place as a result of the constriction, we define a Deborah number for the constriction

$$De_c = \frac{64\tau Q}{\pi R_u^3} = 64De_u. \quad (6)$$

The factor of 64 arises from the faster flow and smaller length scale in the constriction. Elastic effects first become important in the constriction when De_c is of order unity. Under these conditions, De_u is small and so there is little deformation, $\mathbf{A} \approx \mathbf{I}$, upstream.

Stresses, and in particular the pressure drop, are non-dimensionalised with the solvent viscous stress $\mu Q/\pi R_u^3$. The magnitude of the non-Newtonian stresses is also controlled by the non-dimensional group which we shall call the ‘concentration’

$$c = G\tau/\mu_s, \quad (7)$$

so that the non-dimensional shear viscosity is $1 + c$. We shall give results in terms of the three nondimensional groups De_c , c and L .

As pointed out by Cartoalos and Piau [2], a particular convenience of the orifice geometry against the 4:1 contraction is the simple relation between the pressure drop and the rate of dissipation. The rate of dissipation is the rate of working against the stress

$$\mathcal{D} = \int_V \boldsymbol{\sigma} : \nabla \mathbf{u} \, dV, \quad (8)$$

where V is the fluid volume. For inertialess flow, the divergence theorem gives

$$\mathcal{D} = - \int_S \mathbf{u} \cdot \boldsymbol{\sigma} \cdot \mathbf{n} \, dS.$$

Now on the solid surfaces $\mathbf{u} = 0$. Far downstream the stress $\boldsymbol{\sigma}$ returns to its value far upstream except for a pressure drop Δp . Hence

$$\mathcal{D} = Q \Delta p. \quad (9)$$

For inertialess conditions this result applies at each instant. The result comes from the exact recovery of the stored elastic energy, unlike that in the 4:1 contraction. We use the result to give improved accuracy in calculation of the pressure drop, by basing the numerical calculation on a variational statement for \mathcal{D} .

3. Numerical method

We use the split Lagrangian–Eulerian finite element method developed by Harlen, Rallison and Szabo [5]. We give only a brief description of the main ideas here.

The numerical procedure consists of two parts. The Eulerian finite element part solves a Stokes flow problem Eqs. (1)–(3) for the velocity \mathbf{u} forced by the instantaneous elastic stress $G\mathbf{A}$. At high deformations this elastic stress in the FENE-fluid behaves more like the viscous stress in a fibre suspension. To improve convergence rates, we use Eq. (4) to combine this viscous part of the stress with that of the solvent

$$-\nabla p + \nabla \cdot [(\mathbf{I} + c\mathbf{A}) \cdot \mathbf{E} + \mathbf{E} \cdot (\mathbf{I} + c\mathbf{A})] = c \nabla \cdot \frac{\mathcal{D}\mathbf{A}}{\mathcal{D}t}, \quad (10)$$

where

$$\frac{\mathcal{D}\mathbf{A}}{\mathcal{D}t} = \frac{\partial \mathbf{A}}{\partial t} + \mathbf{u} \cdot \nabla \mathbf{A} - \mathbf{A} \cdot \boldsymbol{\Omega} + \boldsymbol{\Omega} \cdot \mathbf{A}$$

is the co-rotational Jaumann derivative with the vorticity tensor $\boldsymbol{\Omega} = \frac{1}{2}(\nabla \mathbf{u} - \nabla \mathbf{u}^T)$. The left hand side of Eq. (10) corresponds to an inhomogeneous anisotropic viscosity $\mu_{ijkl} = (\delta_{ik} + c\mathbf{A}_{ik})\delta_{jl} + \delta_{ik}(\delta_{jl} + c\mathbf{A}_{jl})$. An important feature of our formulation is the symmetry $\mu_{ijkl} = \mu_{klij}$ which ensures the discretised problem is also symmetric.

Triangular elements are used with linear approximations to the velocity and pressure, and with the deformation \mathbf{A} taken to be a constant. This does not fulfil the Brezzi–Babūška condition [1], so to suppress spurious pressure modes the incompressibility condition is modified to

$$\nabla \cdot \mathbf{u} = \beta h^2 \nabla^2 p. \quad (11)$$

Here $\beta = 0.025$ optimally [10,11] and h^2 is twice the area of a triangle. The resulting system of sparse algebraic equations is solved by a preconditioned conjugate gradient method.

The Lagrangian part of the program integrates Eq. (4) in time to obtain the evolution of the deformation \mathbf{A} . By advecting the triangles with the flow \mathbf{u} , we subsume the hyperbolic $\mathbf{u} \cdot \nabla \mathbf{A}$

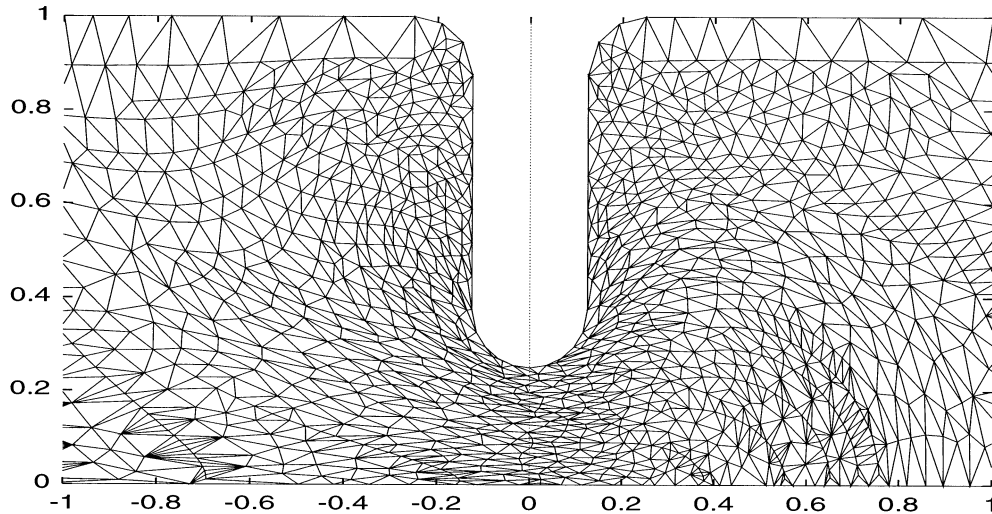


Fig. 2. Deformed mesh of 3818 elements at $t = 0.79$ for $c = 8$, $L = 5$ and $De_c = 9.6$. The full grid extends between $z = \pm 5$.

term. For the co-deformational time derivative on the left hand side of Eq. (4), we resolve \mathbf{A} , which is constant over the element, onto base vectors formed from the edges of the triangle, and then deform \mathbf{A} with the triangle. It then remains to relax \mathbf{A} according to the right hand side of Eq. (4). Using a first order fully implicit scheme, a time-step around 2×10^{-4} could be used. With a mesh of 3818 elements (5555 degrees of freedom), one time step took about 30 s on an HP-735.

The Lagrangian approach of advecting the triangles with the flow suffers from two problems: the triangles become very distorted and regions of the flow become crowded or depleted of triangles. The distortion of the triangles is limited by reconnecting nodes at each time-step according to a Delaunay technique modified to take into account the anisotropy of \mathbf{A} [5]. Nodes are added and removed in order to keep high resolution in the constriction, where there are large gradients of stress, and to reduce the computational effort for regions of little activity. Fig. 2 shows a typical mesh after it has been advected with the flow and nodes have been reconnected and relocated.

This method has been shown to give correct results for the benchmark problem of a sphere in a tube up to a Deborah number of order unity [5]. For our geometry we do not know of other numerical results with which to compare. We checked that pressure drop for a Stokes flow showed a h^2 -convergence with mesh refinement, changing from 912 to 8450 elements. We also found approximate h^2 -convergence for the pressure drop at $De_c = 1.28$. It seems that an accuracy of about 3% can be obtained for the pressure drop with our grid of 3818 elements.

4. Steady results

Setting the concentration c to zero, we obtain the Stokes flow for the pure viscous solvent. The total pressure drop Δp (non-dimensionalised by $\mu Q/\pi R_u^3$) for the pipe running from $z = -5$ to $z = 5$ (non-dimensionalised by the radius of the upstream pipe R_u) is found to be 103 for the rounded constriction ($n = 2$) and 120 for the sharper, longer ($n = 4$) constriction. These values should be compared with that of 80 for an unstricted pipe of length 10. Thus the constrictions enhance the pressure drop only modestly, equivalent to extending the pipe by just 2.9 and 5 radii respectively. An attempt to predict these enhancements using an integral of the hydraulic radius failed because the radius changes too abruptly.

The Stokes flow has vortices symmetrically up and downstream of the constriction. The downstream vortex is shown in Fig. 3a. These vortices are essentially corner vortices, starting roughly midway between the outer wall and the lip of the constriction, near $r = 0.53$, and extending away from the plate at $z = 0.125$ to about $z = 0.375$.

For weakly non-Newtonian flows, $De_c < 1/2$, the flow changes little from the Stokes flow. It remains symmetric up and downstream of the constriction. The microstructure \mathbf{A} is perturbed slightly from the rest value \mathbf{I} , and these perturbations are also symmetric, because at low De_c they are proportional to the local strain-rate. The perturbations to \mathbf{A} do augment the viscosity of the solution to $(1 + c)$ times the solvent viscosity. Hence the pressure drop increases to $103(1 + c)$ and $120(1 + c)$ for the rounder and sharper constrictions respectively.

As the Deborah number in the constriction De_c is increased further, the downstream vortex diminishes and then vanishes. Fig. 3b shows the flow downstream of the constriction for

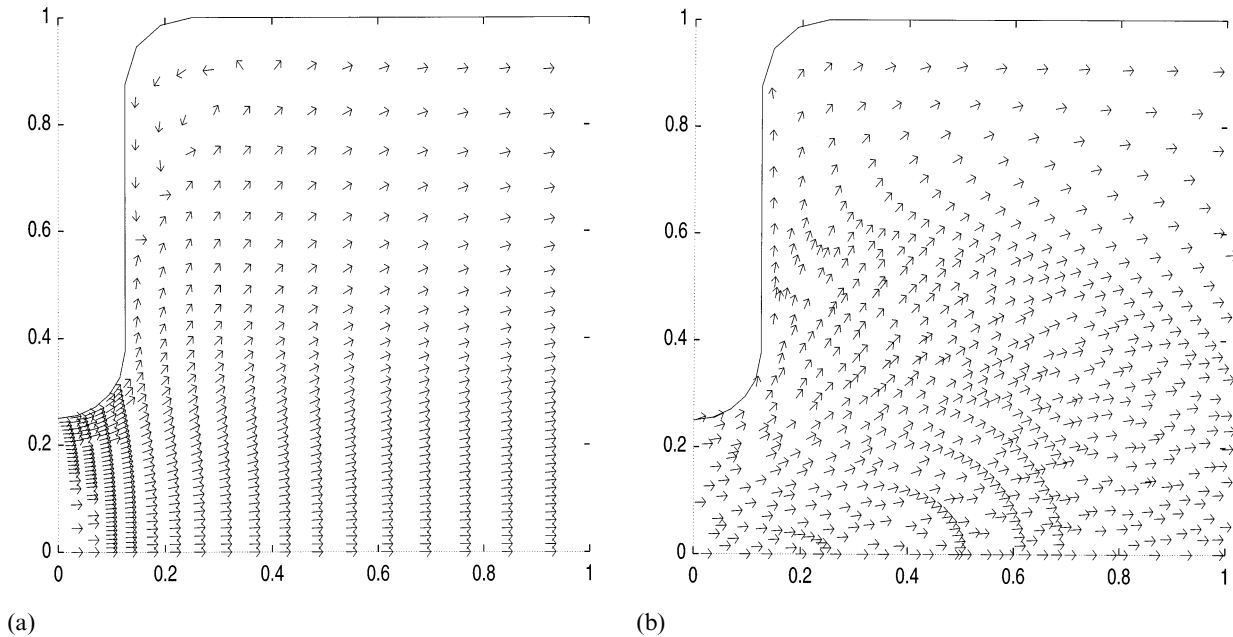


Fig. 3. The downstream vortex, (a) for the Stokes flow $c = 0$, and (b) for the moderately non-Newtonian flow $De_c = 3.2$, $c = 8$ and $L = 5$.

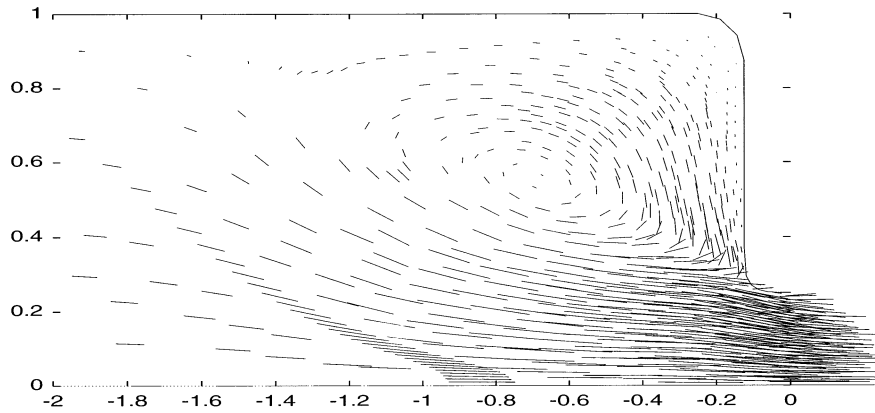


Fig. 4. The upstream vortex for the $De_c = 9.6$, $c = 8$ and $L = 5$. The length of the lines is proportional to $\ln(1 + v)$.

$De_c = 3.2$, $c = 8$ and $L = 5$. There is no longer a vortex. It appears that downstream of the constriction the recovery of the elastic stress pushes the flow outward, as in die swell, and this suppresses the vortex.

Upstream of the constriction, the vortex grows slightly as the Deborah number is increased to about 1, and then begins to grow more strongly. Fig. 4 shows a large upstream vortex at $De_c = 9.6$, $c = 8$ and $L = 5$. In this figure, the length of the lines has been made proportional to $\ln(1 + v)$ in order to show simultaneously the fast flow through the orifice together with the slow recirculation flow in the vortex. The vortex stretches from the plate at $z = -0.125$ upstream to about $z = -1.45$.

The growth and development of the upstream vortex is represented in Fig. 5 by the change of the flow attachment points and the centre of the vortex as the Deborah number De_c is increased. The detachment point does not move until $De_c = 1.3$, when it begins to move upstream. On the other hand, the re-attachment point moves immediately from mid-way along the constriction plate, arriving at the lip of the constriction by $De_c = 3.2$ and then remaining there. The centre of the vortex first moves gradually out of the corner as the vortex fills the corner, and then at $De_c = 3.2$ starts to move upstream as the vortex elongates.

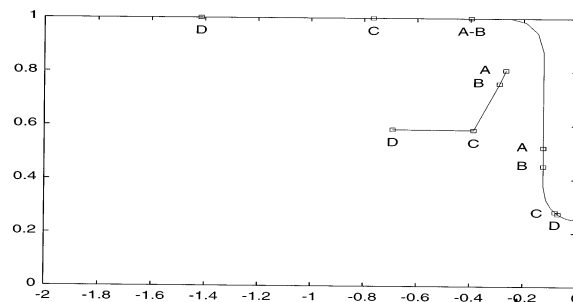


Fig. 5. The position of the centre of the vortex and the detachment and re-attachment points of the streamline around the vortex: A for $De_c = 0$; B for $De_c = 1.28$; C for $De_c = 3.2$; D for $De_c = 9.6$; all with $c = 8$ and $L = 5$.

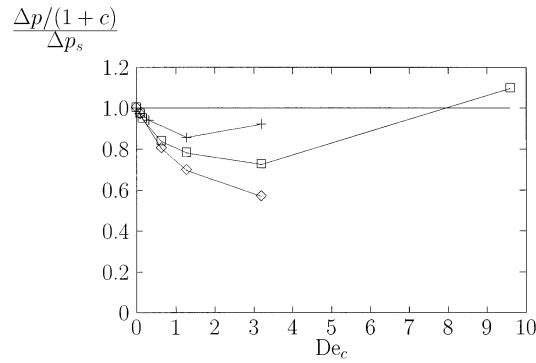


Fig. 6. The change in the pressure drop Δp with Deborah number De_c , for $c = 8$, and \diamond for $L = \infty$, \square for $L = 5$, and $+$ for $L = 3.26$.

The variation of the pressure drop with Deborah number is shown in Fig. 6. The pressure drops here have been divided by the low Deborah number value $103(1+c)$. Setting the finite extensibility L equal to a very large number, we recover the results for the Oldroyd-B fluid. This has a pressure drop that decreases steadily with Deborah number. By $De_c = 3.2$ the pressure drop is equivalent to a pipe of length 8 without a constriction, using the steady viscosity $(1+c)$ times the solvent viscosity. Note that the Deborah number in the upstream pipe is $De_c = 0.05$, so that the elastic stress is little perturbed and is fully relaxed at the outlet and inlet. The explanation for the large reduction in pressure drop lies in the transient nature of the flow seen by moving fluid elements. The viscosity attains its steady value $(1+c)$ only after experiencing a strain-rate for the duration of the relaxation time. Hence in the convergence into the constriction the non-dimensional viscosity is less than $(1+c)$.

With a finite extension limit L , the pressure drop initially decreases, reaches a minimum, and then increases with increasing Deborah number. At sufficiently large Deborah number, the pressure drop exceeds that for a Newtonian fluid having viscosity $(1+c)$. In the fast converging flow into the constriction, the FENE fluid behaves viscously with a high (Trouton) extensional viscosity $(3+2cL^2)$ times the solvent viscosity, and this viscous response increases the dissipation and hence the pressure drop. There is an interesting trade-off here in which small finite extensions L have a smaller (Trouton) extensional viscosity $(3+2cL^2)$ but need less stretch to attain the extension L , and so become effective first at lower Deborah numbers.

The pressure drop, relative to the Newtonian drop with viscosity $(1+c)$, was found to be insensitive to the rounding of the corner, comparing the corner $n = 2$ with $n = 4$. A modification of the constitutive equation to reflect an increase with the deformation of the frictional grip on the beads of the dumbbell was also found to have no interesting effect.

5. Start-up results

We now consider how the steady state is established starting from an undeformed initial microstructure, $\mathbf{A} = \mathbf{I}$. Fig. 7 shows the build-up in the pressure drop for the strongly non-New-

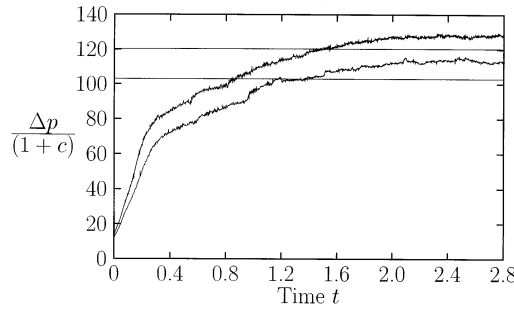


Fig. 7. The build-up of the pressure drop Δp divided by $(1+c)$ for $De_c = 9.6$, $c = 8$ and $L = 5$. The lower curve corresponds to the rounded corner $n = 2$ while the upper curve corresponds to the sharper corner $n = 4$.

tonian flow with $De_c = 9.6$. The small fluctuations arise from the regridding which is made at each time-step. Initially with no deformation, there is no elastic contribution to the stress, and so the response is just that of the Newtonian viscous solvent. Hence the initial (non-dimensional) pressure drops are 103 and 120 for the rounded and sharper corners respectively. At $De_c = 9.6$, the steady pressure drops are a little larger than $103(1+c)$ and $120(1+c)$, which are approached by the time $t = 3.0$. The interesting feature in the transient response is the transition at $t = 0.2$ between a fast phase with a rapid increase, and a second phase with a much slower, by a factor of 5, increase in the pressure drop.

The growth in time of the vortex can be seen in Fig. 8 by the changing positions of the centre of the vortex and the flow attachment points. The vortex starts as a small Newtonian corner vortex. When the flow starts, the re-attachment point moves steadily along the constriction plate, reaching the lip of the constriction at $t = 0.2$ and then remaining fixed. During this time, the detachment point moves upstream from $z = -0.4$ to -0.65 , and the centre of the vortex moves mainly towards the axis of the pipe. After $t = 0.2$ the vortex gradually lengthens, the detachment point moving upstream to $z = -1.45$ by $t = 1.3$. During this time the centre of the vortex also moves upstream, from $z = -0.35$ to -0.75 . The clear change in direction of the motion of the centre of the vortex occurs precisely when the pressure drop changes from rapid to slow growth.

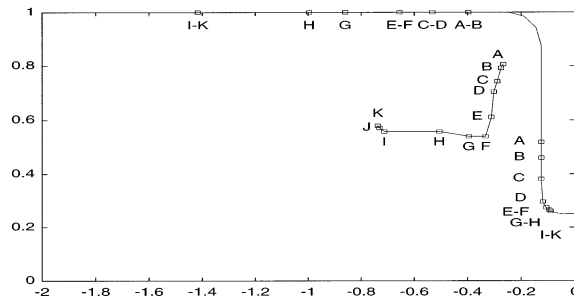


Fig. 8. The motion of the centre of the vortex and the detachment and re-attachment points of the streamline around the vortex for $De_c = 9.6$, $c = 8$ and $L = 5$. The labeled points correspond to different times: A, $t = 0$; B, $t = 0.05$; C, $t = 0.1$; D, $t = 0.15$; E, $t = 0.2$; F, $t = 0.25$; G, $t = 0.35$; H, $t = 0.55$; I, $t = 1.37$; J, $t = 2.17$; K, $t = 2.82$.

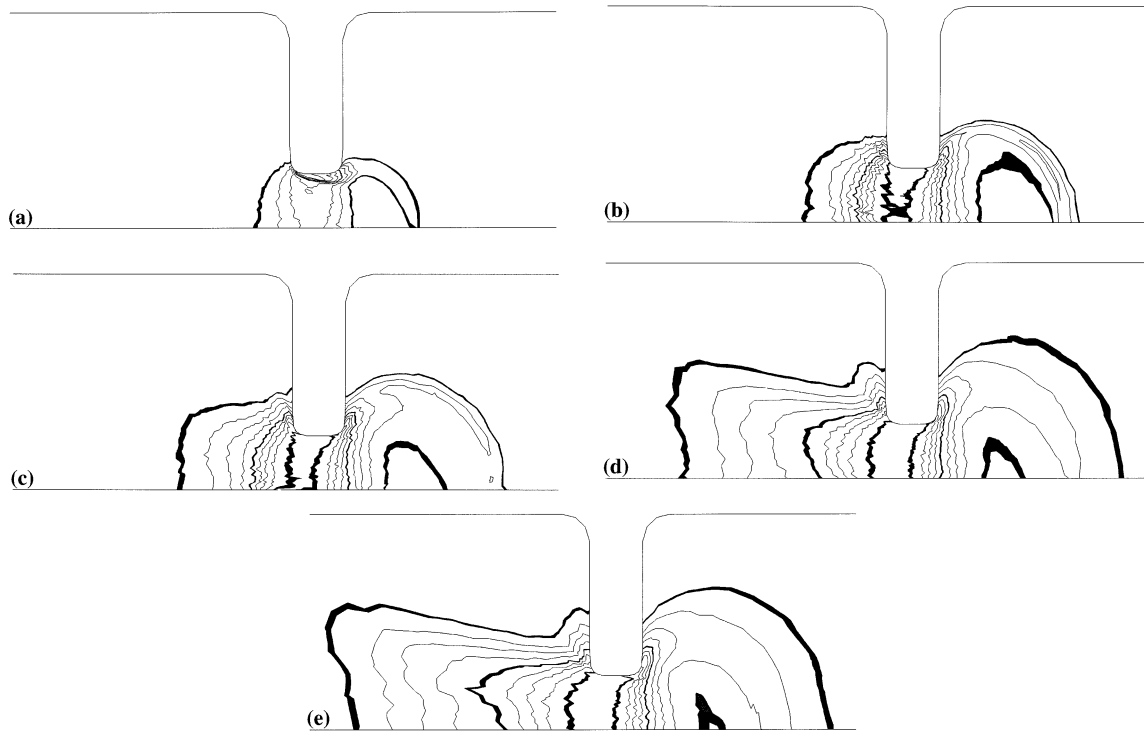


Fig. 9. Contour plots of $\text{trace}(\mathbf{A})$ at different times; (a) for $t = 0.1$, (b) for $t = 0.35$, (c) for $t = 0.55$, (d) for $t = 1.37$ and (e) for $t = 2.82$. The thick contours mark where $\text{trace}(\mathbf{A})$ lies between 6 ± 0.15 , 15 ± 0.15 and 21 ± 0.15 . The thin contours are equally spaced between. The flow has $De_c = 9.6$, $c = 8$ and $L = 5$.

The build-up of the deformation of the microstructure can be seen in Fig. 9, where we give at different times contour plots of $\text{trace}(\mathbf{A})$. At $t = 0.1$ in Fig. 9a, the material is most stretched by the high shear on the surface of the constriction. Note the region downstream of the constriction where the divergence has unwound the strain in the converging flow upstream, leaving the microstructure fairly undeformed. By $t = 0.35$ in Fig. 9b, the material is stretched to $\text{trace}(\mathbf{A}) = 15$ uniformly across the neck of the constriction. The position of $\text{trace}(\mathbf{A}) = 6$ has moved upstream a little, and the region of unwound undeformed material has moved downstream a little. By $t = 0.55$ in Fig. 9c, the deformation in the neck of the constriction has reached 21, which is nearing the maximum extension $L^2 = 25$, but the pattern remains unchanged. In the final two in Fig. 9d and 9e corresponding to $t = 1.37$ and 2.82, we see the vortex growing upstream, with the deformation changing little elsewhere. Note the deformation is small in the recirculating vortex, and is fairly uniform across the converging cone.

6. A simple model of the upstream vortex and its growth

Our aim in this section is to offer scaling estimates for the size of the upstream vortex and its growth. In this section we revert to dimensional variables.

In the first phase while the vortex remains in the corner, we model the converging flow into the constriction very crudely as the flow into a point sink,

$$u = -\frac{Q}{2\pi r^2}. \quad (12)$$

We here use the symbol r for the distance from an effective origin in the entrance to the constriction. This model of a point-sink flow applies for distances larger than the radius of the constriction and less than the radius of the upstream pipe, $R_c < r < R_u$.

Now the microstructure \mathbf{A} associated with a fluid element starts to deform significantly once the strain-rate $E = \partial u / \partial r = Q / \pi r^3$ that it experiences exceeds half the relaxation rate $1/2\tau$. Thus all the material in

$$r < r_D = (2Q\tau/\pi)^{1/3} = R_c(2De_c)^{1/3}$$

begins to stretch when the flow is switched on. For $De_c = 9.6$, $r_D = 2.7R_c$. This model is appropriate only if r_D lies inside the radius of the upstream pipe, $4R_c$ for our computations. The case of $r_D > R_u$ only occurs when $De_u > 1/2$. For our 4:1:4 constriction, $De_u = 0.15$ when $De_c = 9.6$.

Moving with the point-sink flow, the material sees a rapidly increasing strain-rate. Hence once it begins to stretch, the relaxation term can be neglected. The material thus stretches like a fluid line-element. So in a steady flow, $A \propto u^2 \propto r^{-4}$.

The first phase of the vortex growth comes to an end if some material reaches the finite extension limit $A = L^2$. This first occurs at the constriction $r = R_c$ with material which started at $r = R_c L^{1/2}$, where the velocity is L^{-1} smaller. We need this starting position to be inside the region $r < r_D$ where material is being stretched, i.e. we need the Deborah number to be sufficiently large $De_c > \frac{1}{2}L^{3/2}$. If the Deborah number does not exceed this critical value, then no material reaches the maximum extension limit. Thus we see in Fig. 5 where $\frac{1}{2}L^{3/2} = 5.6$ that the vortex remains near the corner for $De_c = 1.28$ and 3.2 , while a large vortex grows for $De_c = 9.6$. Further, in Fig. 6 we see that the steady pressure drop has just begun to increase from its minimum at $De_c = \frac{1}{2}L^{3/2}$, i.e. at $De_c = 2.9$ for $L = 3.26$ and at $De_c = 5.6$ for $L = 5$.

Returning to the material which starts at $r = R_c L^{1/2}$, the time it takes to reach the constriction $r = R_c$ moving in the point-sink flow Eq. (12) is

$$t_1 = \frac{2\pi R_c^3}{3Q}(L^{3/2} - 1).$$

In scaling terms, this is the time to move the distance $R_c L^{1/2}$ at the velocity $Q/2\pi R_c^2 L$ of the sink at that distance from the effective origin. This then gives the duration of the first phase, during which the vortex remains in the corner. For the conditions of Fig. 7 giving the build up of pressure in time, we predict the duration of the first phase as $0.1\pi R_u^3/Q$, or 0.1 in the non-dimensionalisation used earlier. This must be compared with the numerical result in the figure of 0.2 in non-dimensional units. The attachment points in Fig. 8 start to move differently at 0.25. Fig. 9a and show that material is fully stretched by 0.35 but not by 0.1.

Once the microstructure is deformed nearly to the finite extension limit, the FENE fluid behaves like a suspension of rigid fibres, i.e. a viscous material (stress proportional to the instantaneous strain-rate) with an anisotropic viscosity. The shear viscosity near to the finite extension limit is the solvent value μ_s , while the (Trouton) extensional viscosity is $3\mu_s + 2G\pi L^2 = 3\mu_s(1 + \frac{2}{3}cL^2)$. For the conditions of the large upstream vortex in Fig. 4, $c = 8$ and $L = 5$, this extensional viscosity is 201 times the shear viscosity. The anisotropy in the viscosity induces an anisotropy in the flow. For the converging flow, Evans [4] and Keiller, Rallison and Evans [8] have shown that the anisotropy takes the form of the inflow being restricted to a small cone of angle $\alpha = c^{-1/2}L^{-1}$, in order that the shear forces $\mu_s \partial^2 u / r^2 \partial \theta^2$ can balance the extensional forces $\mu_s(1 + \frac{2}{3}cL^2) \partial^2 u / \partial r^2$. For the conditions in Fig. 4, $\alpha = 0.07$. Outside this narrow cone is the recirculating vortex with much smaller deformations, see Fig. 9e. It is difficult to estimate a precise cone angle for Fig. 4, but as measured near $z = -0.5$ an angle of about 0.13 might be more appropriate than 0.07.

As a very simple model of the fully developed steady upstream vortex, we propose a narrow-angled cone containing highly stretched material which will pass through the constriction. Outside this narrow cone is less-stretched material in the recirculating eddy. The cone has a finite length and terminates before reaching the outer wall if the Deborah number based on the upstream pipe is small, $De_u < 1$. We model the converging flow into the base of this narrow cone as a point-sink flow again, but now with an effective origin now in the base of the cone, see Fig. 10. The flow as a whole therefore has the appearance of a wine glass, having a narrow conical stem surmounted by a wide angled bowl.

Now, in the point-sink flow, material starts to stretch at $r = r_D = R_c(2De_c)^{1/3}$, and, stretching like a fluid line-element, $A \propto u^2 \propto r^{-4}$, becomes fully stretched at $r = R_c(2De_c)^{1/3}L^{-1/2}$. Once this material is fully stretched, it ceases to be part of the point-sink flow and enters the narrow cone, hence the value of r gives the radius of the cone at its base. Noting that we are in a regime where $De_c > \frac{1}{2}L^{3/2}$ in order that material can be stretched to near its finite extension limit, the model consistently requires that the radius at the entrance be greater than that of the constriction. The rate at which the cone tapers is of course the cone angle α . Taking this to be $c^{-1/2}L^{-1}$, we predict the length of the cone to be

$$H(\infty) = R_c((2De_c)^{1/3}L^{-1/2} - 1)c^{1/2}L. \quad (13)$$

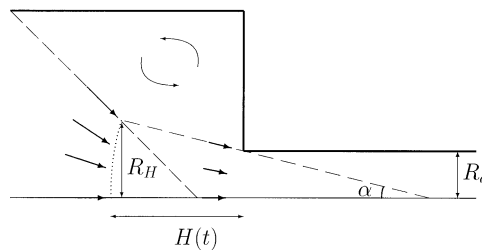


Fig. 10. Simple model of the wine

shape of the upstream vortex, with long narrow cone fed into its base by a point-sink flow.

The length of the vortex will be larger due to the wide angled bowl feeding the narrow cone. If we arbitrarily set this wide angle to be 45°, then we need to add $R_u - R_c(2De_c)^{1/3}L^{-1/2}$. For the conditions in Fig. 4, this contribution is $0.7R_u$ to be added to $H(\infty) = 0.7R_u$. The prediction of $1.4R_u$ for the length of the vortex to the detachment point of the streamline around it compares favourably with the numerical result of $1.32R_u$.

We now consider the second phase of the evolution of the vortex. At the end of the first phase, there is fully stretched material just at the entrance to the constriction. During the second phase, we propose as a simple model that there is fully stretched material within a narrow cone of length $H(t)$, which grows gradually from the constriction until it has the fully developed length given by Eq. (13). The flow into the entrance of the growing cone is a point-sink flow with an effective origin in the current entrance. The rate at which the length of the cone grows \dot{H} is such that material arriving at the entrance has just been stretched to the finite extension limit.

The key to the calculation of the growth of the cone \dot{H} is to determine the position where the velocity of the point-sink flow Eq. (12) is equal to \dot{H} , i.e. $r = r_{\dot{H}} = (Q/2\pi\dot{H})^{1/2}$. At larger distances, the changes due to the advancing cone dominate those arising from the deformation in the point-sink flow. On the other hand, at smaller distances, material moves rapidly in the point-sink flow, which can be regarded as steady. We will soon find that this critical distance is within the region where material is significantly stretched, $r_{\dot{H}} \leq r_D$. At distances $r_{\dot{H}} < r < r_D$, the strain-rate is smaller than the rate at which it is changing due to the advancing cone, and so the material is stretched little while it remains in this region. At distances $r < r_{\dot{H}}$, the material is stretched by the quasi-steady point-sink flow, so that $A \propto u^2 \propto r^{-4}$. It therefore becomes fully stretched at $r = r_{\dot{H}}L^{-1/2}$. This must be the radius of the current entrance to the cone, $R_H(t)$ say. Thus we have determined the velocity at which the cone must grow

$$\dot{H} = \frac{Q}{2\pi R_H^2 L}. \tag{14}$$

This velocity is much smaller than the velocity of the material entering the cone, $Q/2\pi R_H^2$.

Now the radius of the entrance to the cone R_H increases from the initial R_c to the final $R_c(2De_c)^{1/3}L^{-1/2}$. As material stretches fully between $r_{\dot{H}}$ and R_H , we deduce that $r_{\dot{H}}$ varies between the initial $R_cL^{1/2}$ and the larger final $R_c(2De_c)^{1/3}$. The latter is r_D . Thus we confirm the earlier assertion that $r_{\dot{H}} \leq r_D$.

The evolution of the length of the cone is finally found from the relation between the radius of the cone $R_H(t)$, its length $H(t)$ and the cone angle $c^{-1/2}L^{-1}$

$$R_H = R_c + H/\alpha$$

and Eq. (14) for the velocity at which the cone grows. Integrating, we find the time to establish the fully developed cone is

$$t_2 = \frac{2\pi R_c^3}{3Q} (2De_c L^{-3/2} - 1) c^{1/2} L^2 \tag{15}$$

Essentially this is the time to grow to the length H given by Eq. (13) at the velocity of the point-sink flow Eq. (12) at $r = r_D$. For the conditions in Fig. 8, this is $0.53\pi R_u^3/Q$ compared with the numerical result of about $1.4\pi R_u^3/Q$.

Acknowledgements

One of the authors (PS) was supported by the EU Human Capital and Mobility Program grant CHRX-CT93-0200 and the Danish Technical Research Council grant number 16-5390-1 PG. The computations were supported in part by the SERC CSI grant GR/H57585.

References

- [1] F. Brezzi, M. Fortin, *Mixed and Hybrid Finite Element Methods*, Springer Verlag, New York, 1991.
- [2] U. Cartalos, J.M. Piau, Creeping flow regimes of low concentration polymer solutions in which solvents through an orifice die, *J. Non-Newtonian Fluid Mech.* 45 (1992) 231–285.
- [3] M.D. Chilcott, J.M. Rallison, Creeping flow of dilute polymer solutions past cylinders and spheres, *J. Non-Newtonian Fluid Mech.* 29 (1988) 382–432.
- [4] J.G. Evans, The effect of the non-Newtonian properties of a suspension of rod-like particles on flow fields, in: J.F. Hutton, J.R.A. Pearson, K. Walters (Eds.), *Theoretical Rheology*, Applied Science Publishers, London, 1975, pp. 224–232.
- [5] O.G. Harlen, J.M. Rallison, P. Szabo, A split Lagrangian-Eulerian method for simulating transient viscoelastic flows, *J. Non-Newtonian Fluid Mech.* 44 (1995) 229–265.
- [6] G.H. McKinley, W.P. Raiford, R.A. Brown, R.C. Armstrong, Nonlinear dynamics of viscoelastic flow in axisymmetric abrupt contractions, *J. Fluid Mech.* 223 (1991) 411–456.
- [7] R.A. Keiller, Entry-flow calculations for the Oldroyd-B and FENE equations, *J. Non-Newtonian Fluid Mech.* 42 (1993) 143–178.
- [8] R.A. Keiller, J.M. Rallison, J.G. Evans, Sink flows of a suspension of rigid rods: the failure of a similarity solution, *J. Non-Newtonian Fluid Mech.* 42 (1992) 249–266.
- [9] J.M. Marchal, M.J. Crochet, A new mixed finite element for calculating viscoelastic flow, *J. Non-Newtonian Fluid Mech.* 26 (1987) 77–114.
- [10] A. Wathen, D. Silvester, Fast iterative solution of stabilised Stokes systems. Part I: Using simple diagonal preconditioners, *SIAM J. Numer. Anal.* 30 (1993) 630–649.
- [11] D. Silvester, A. Wathen, Fast iterative solution of stabilised Stokes systems. II: Using general block preconditioners, *SIAM J. Numer. Anal.* 31 (1994) 1352–1367.